Supporting Information

Distorted MO$_6$ octahedral unit on the activity and stability for the oxygen evolution reaction

Haixiang Yang[‡a], Xinran Ning[‡a], Wenjun Yan[a], Hua Gui Yang[a], Haiyang Yuan*[a]
[a]Key Laboratory for Ultrafine Materials of Ministry of Education, Shanghai Engineering Research Center of Hierarchical Nanomaterials, School of Materials Science and Engineering, East China University of Science and Technology, Shanghai 200237, China

Note S1. Computational Method

All the spin-polarized calculations were performed using the Vienna Ab-initio Simulation Package (VASP) package[1-3]. The exchange-correlation functional was described by the Perdew-Burke-Ernzerhof (PBE) functional[4] within the generalized gradient approximation (GGA)[5]. The project-augmented wave (PAW) method[6] was employed to treat core electrons, and the cutoff energy of plane-wave basis was set to 450 eV. We constructed $p(2\times1)$ rutile-MO_2 (110) surfaces (M = Cr, Mn, Rh, Ru and Ir), and a vacuum layer of 15 Å was applied to separate each periodic unit cell. The Brillouin zone was sampled by $3 \times 3 \times 1$ Monkhorst-Pack mesh k-points for all structure optimizations. In the process of structure optimization, the bottom 2 layers of atoms were fixed. In order to accurately describe the electron correlation in the localized d-orbital of metal ions in $3d$ transition metal oxides, the DFT + U method was adopted[7]. The specific applied U_{eff} values (U_{eff} = U-J) are shown in Table S1. Here, all Gibbs free energy (ΔG) change includes the zero-point energy (ΔZPE) and entropy ($T\Delta S$) corrections, calculated as $\Delta G = \Delta E + \Delta ZPE - T\Delta S$, where ΔE is the energy obtained from DFT optimization. The calculation of ZPE and TS involves performing a frequency calculation on the optimized molecule or adsorbed species, and then they are derived from the standard partition functions[8]. Notably, the entropy contribution of the reactant or product molecule is obtained from the experimental value[9].

Table S1 The specific applied U value (U_{eff}) of $3d$ metals for DFT calculations[7].

$3d$	Cr	Mn	Co	Ni
U_{eff}	2.79	3.06	3.42	3.4

**Note S2. Calculation of dissolution energy (ΔG_d) of metal center**

To assess the stability of metal center in MO_6 incorporated in rutile metal oxides, the dissolution energy (ΔG_d) of metal center was calculated, which can be taken as the standard to determine the stability of MO_6. The dissolution of metal center in MO_6 can be displayed as follows:

sur-M + xH$_2$O $\rightarrow$ sur-vac + MO$_x$ + $2x$(H$^+$/e$^-$)
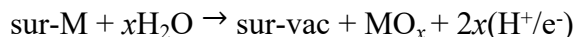
The specific dissolution energy (ΔG_d) of metal center can be written as:

$\Delta G_d = G(\text{sur-vac}) + G(\text{MO}_x) + 2xG(\text{H}^+/\text{e}^-) - G(\text{sur-M}) - xG(\text{H}_2\text{O})$

in which $G(\text{sur-M})$ and $G(\text{sur-vac})$ correspond to the energy of the perfect surface with M involved and the defective surface after M dissolves. $G(\text{H}_2\text{O})$ is the free energy of H$_2$O molecule (T = 298 K). $G(\text{H}^+/\text{e}^-)$ is the free energy of proton and electron (H$^+$/e$^-$), which is obtained by referencing it to the free energy of H$_2$ using the computational standard hydrogen electrode at U= 0 V vs. SHE (pH = 0, T = 298 K) and including a -eU term from an external potential U. $G(\text{MO}_x)$ is the energy of the dissolved product. The dissolved or converted compounds of different metal elements are obtained from the Pourbaix diagram of Materials Project at U = 1.5 V (vs. SHE) and pH = 0. When MO$_x$ is solid, its energy is obtained from the total energy of its bulk. As MO$_x$ is an ionic compound, its energy is calculated with the Pourbaix diagram in Materials Project. Taking RuO$_4$·H$_2$O$_{(aq)}$ as the example, we used the Pourbaix diagram of RuO$_{2(s)}$ as the standard and calculated $G(\text{RuO}_4\cdot\text{H}_2\text{O}_{(aq)})$ by following equation:

RuO$_4$·H$_2$O$_{(aq)}$ + 4H$^+$ + 4e$^-$ $\rightarrow$ RuO$_{2(s)}$ + 3H$_2$O
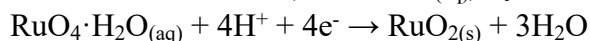
$G(\text{RuO}_4\cdot\text{H}_2\text{O}_{(aq)}) = G(\text{RuO}_{2(s)}) + 3G(\text{H}_2\text{O}) - 2G(\text{H}_2) - \Delta G$
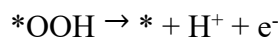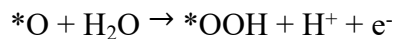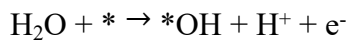
where ΔG is the phase transition energy of RuO$_4$·H$_2$O$_{(aq)}$ + 4H$^+$ + 4e$^-$ $\rightarrow$ RuO$_{2(s)}$ + 3H$_2$O obtained from the Pourbaix diagram. $G(\text{RuO}_{2(s)})$ is the total energy of the bulk of RuO$_2$ resulting from the DFT calculation. Energies of other ionic compounds were calculated in a similar way. The dissolution/conversion products and related energies (i.e., $G(\text{MO}_x)$) in this work are listed in Table S2.

Table S2 Dissolution products (MO_x) and the free energy ($G(MO_x)$) of metal center at $U = 1.5$ V (vs. SHE) and pH = 0.

M	MO_x	$G(MO_x)$ / eV
Cr	$HCrO_4^-{}_{(aq)}$	-40.07
Mn	$MnO_{2(s)}$	-21.43
Co	$CoO_{2(s)}$	-17.23
Ni	$Ni^{2+}{}_{(aq)}$	-3.25
Ru	$RuO_4 \cdot H_2O_{(aq)}$	-46.32
Ir	$IrO_4^{2-}{}_{(aq)}$	-32.64

Note S3. Calculation of OER overpotential

To assess the activity of oxygen evolution reaction (OER), the general reaction mechanism of OER was considered as follows[10-12]:

$$H_2O + * \rightarrow *OH + H^+ + e^-$$

$$*OH \rightarrow *O + H^+ + e^-$$

$$*O + H_2O \rightarrow *OOH + H^+ + e^-$$

$$*OOH \rightarrow * + H^+ + e^-$$

where * represents the active site, and *OH, *O and *OOH are the adsorbed OH, O and OOH, respectively. The OER activity is evaluated by calculating the overpotential. Firstly, we calculated the free energy of each elementary reaction in OER, and the free energies of the above four steps are written as:

$$\Delta G_1 = G_{[*OH]} - eU - k_bT(\ln10) \times \text{pH}$$

$$\Delta G_2 = G_{[*O]} - G_{[*OH]} - eU - k_bT(\ln10) \times \text{pH}$$

$$\Delta G_3 = G_{[*OOH]} - G_{[*O]} - eU - k_bT(\ln10) \times \text{pH}$$

$$\Delta G_4 = 4.92 - G_{[*OOH]} - eU - k_bT(\ln10) \times \text{pH}$$

$G_{[X]}$ (X = *OH, *O and *OOH) is the adsorption Gibbs free energy of the corresponding oxygen-containing intermediate, which have included the zero-point energy (ΔZPE) and entropy correction ($T\Delta S$). $G_{[X]}$ were calculated relative to H_2O and H_2 at $U = 0$ V (vs. SHE), pH = 0 and $T = 298$ K. Due to the difficulty of GGA-DFT in calculating the bond energy of O_2, the experimental formation energy of two H_2O molecules (4.92 eV) was used to calculate the energy of O_2. The free energy of proton and electron (H^+/e^-) is obtained by referencing it to the free energy of H_2 using the computational standard hydrogen electrode at $U = 0$ V, pH = 0 and $T = 298$ K. In addition, the effect of pH on the reaction was taken into account; $k_bT(\ln10) \times \text{pH}$ term is introduced to correct the error caused by pH change. The theoretical overpotential η of OER can be obtained by comparing and analyzing the steps with the largest free energy values. The calculation formula of overpotential η is as follows:

$$\eta = \text{Max}[\Delta G_1, \Delta G_2, \Delta G_3, \Delta G_4,]/e - 1.23$$
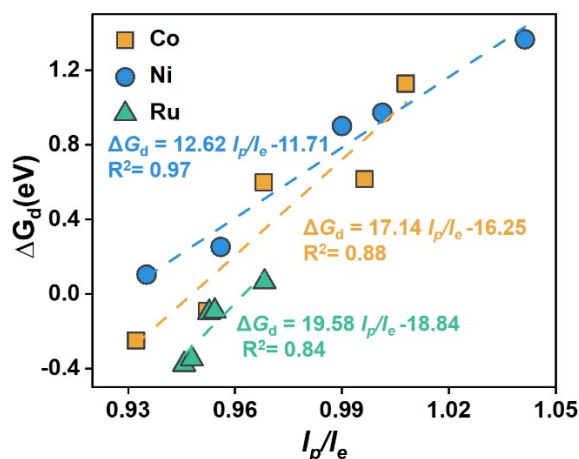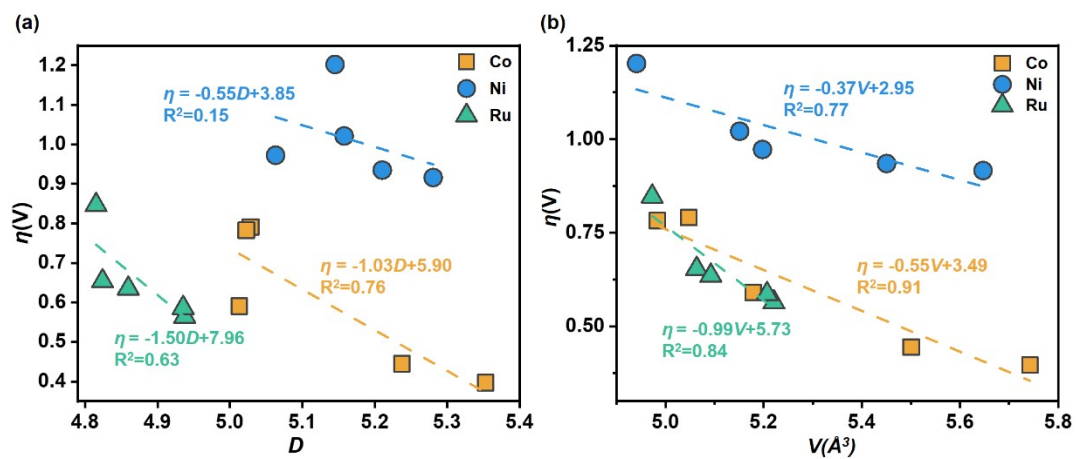
Fig. S1 Relationship of the dissolution free energy (ΔG_d) of metal site as a function of l_p/l_e of MO_6 octahedron (M = Co, Ni, Ru).

Analysing the D value, it can be that the change in D of the MO_6 octahedron mainly comes from the equatorial M-O bonds of MO_6 (l_e, indicated by black values in Fig. 2b), while the polar M-O bonds (l_p, indicated by orange values in Fig. Fig. 2b) undergo relatively small changes. It can be expected that l_p/l_e could also has a relatively good correlation with stability of the MO_6 octahedron. To further verify the correlation between stability and l_p/l_e, we scaled the dissolution free energy (ΔG_d) of MO_6 as a function of l_p/l_e (Fig. S1), and found a relatively good relationship between the CoO_6, NiO_6, and RuO_6 units. As l_p/l_e increases, ΔG_d becomes more positive, indicating improved stability.
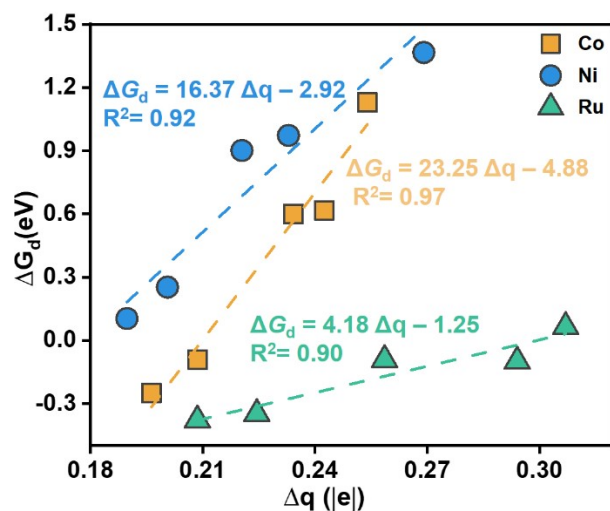
Fig. S2 Relationships between the dissolution free energy (ΔG_d) of metal center of MO_6 and the number of electrons (Δq) transferred from the metal center of MO_6 (M=Co, Ni, Ru) to the surrounding O atoms.

(a)

$\eta = -0.55D+3.85$
$R^2=0.15$

$\eta = -1.03D+5.90$
$R^2=0.76$

$\eta = -1.50D+7.96$
$R^2=0.63$

- Co
- Ni
- Ru

$\eta(V)$

D

(b)

$\eta = -0.37V+2.95$
$R^2=0.77$

$\eta = -0.55V+3.49$
$R^2=0.91$

$\eta = -0.99V+5.73$
$R^2=0.84$

- Co
- Ni
- Ru

$\eta(V)$

$V(Å^3)$

Fig. S3 Relationships of the overpotential η and (a) D and (b) V of CoO_6, NiO_6 and RuO_6 incorporated in different rutile metal oxides, respectively.
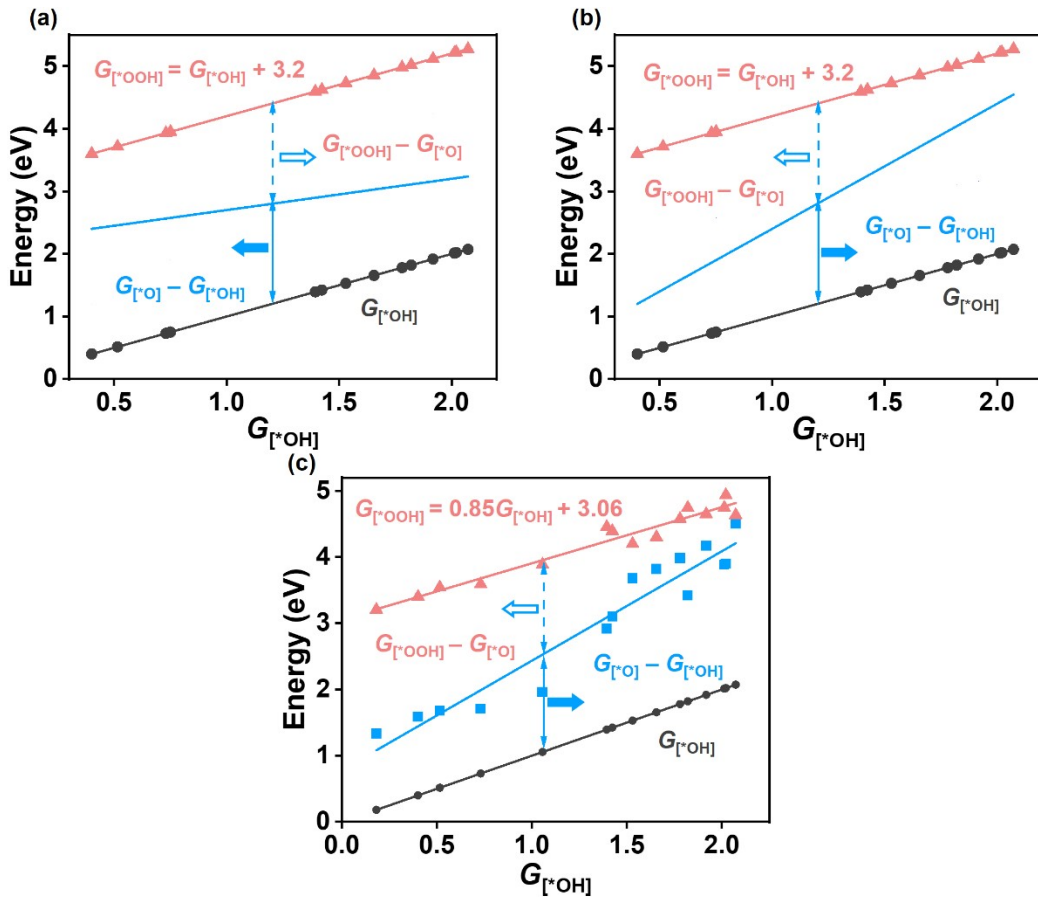
Fig. S4 (a, b) Relationships of adsorption free energies ($G_{[X]}$) of the key intermediates (X = *OH, *O and *OOH) of OER on standard rutile or perovskite oxides, in which the blue lines represent the relationship between $G_{[*O]}$ and $_{[*OH]}$. (a) represent the condition that the slope (α) of the relationship between is less than 1.0; (b) represent the condition that the slope (α) of the relationship between is greater than 1.0. (c) Relationships of $G_{[X]}$ on the distortion of MO_6 upon incorporation into different rutile metal oxides.

Regarding the boundary between the four rate-determining steps, we have marked them with the dash black line, as shown in Fig. 3b. From Fig. 3b, we can find that as the adsorption strength of metal site is weak, resulting in the difficult activation of H_2O, the H_2O deprotonation is rate-determining. With the increase of the binding strength of metal site, the rate-determining step changes to the further *OH deprotonation (*OH → *O + H^+/e^-) or the O-O coupling step (*O + H_2O → *OOH + H^+/e^-). At standard rutile or perovskite oxides, there is a universal scaling relationship between the adsorption energies of *OOH and *OH, $G_{[*OOH]}=G_{[*OH]}+(3.2\pm0.2)$[13], and the gap between $G_{[*OOH]}$ and $G_{[*OH]}$ is a constant. Thus, the slope (α) of the relationship between the adsorption energies of *OH and *O determines the rate-determining step of *OH → *O + H^+/e^- or *O + H_2O → *OOH + H^+/e^-. As α is less than 1.0 (see the blue solid line, Fig. S4a), at the range of the weak adsorption strength of metal site, the rate-determining step is *OH → *O + H^+/e^-; as the adsorption strength of metal site increases to some extent, the rate-determining step changes to *O + H_2O → *OOH + H^+/e^-. As α is greater than 1.0 (see the blue dashed line, Fig. S4b), the contrary tendency can be obtained, and the step of *O + H_2O → *OOH + H^+/e^- could become rate-determining first when the adsorption strength of metal site is relatively weak. Here, as a

consequence of the distortion of MO_6 upon incorporation into different rutile metal oxides, we can find a deviation from the dependence with a smaller slope of 0.85 ($G_{[*OOH]}=0.85G_{[*OH]}+3.06$, $R^2=0.95$, see the red line in Fig. S4c) compared to the universal scaling relationship observed in standard MO_6 in rutile or perovskite oxides. Combining with the relationship between $G_{[*O]}$ and $G_{[*OH]}$ ($G_{[*O]}=1.65G_{[*OH]}+0.78$, $R^2=0.94$, see the blue line in Fig. S4c), one can see that at the adsorption strength of metal site of MO_6 incorporated in rutile metal oxides is relatively weak, the rate-determining step is $*OH \rightarrow *O + H^+/e^-$, and gradually changes to $*O + H_2O \rightarrow *OOH + H^+/e^-$ with the increase of the adsorption strength. When the binding strength of metal site increases to some extent, the conversion of $*OOH$ ($*OOH \rightarrow O_2 + H^+/e^-$) will become rate-determining for the too strong adsorption of $*OOH$ at that time.
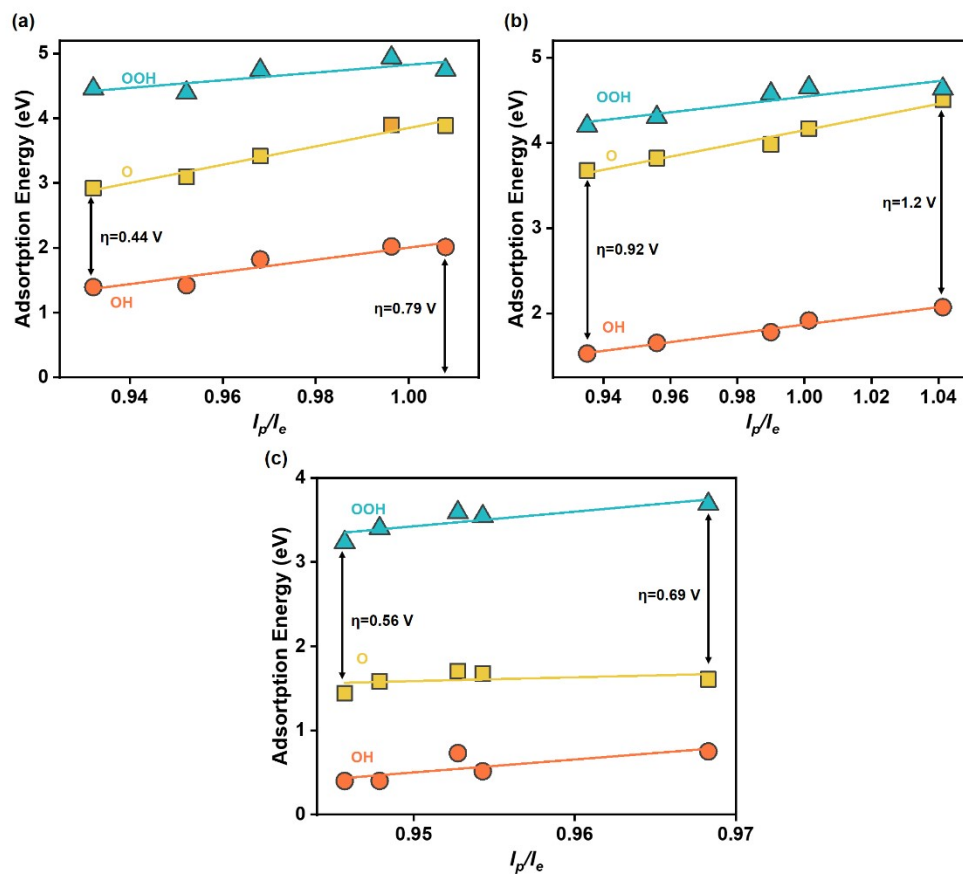
Fig. S5 Correlation of adsorption energies of *OH, *O and *OOH with l_p/l_e of (a) CoO_6, (b) NiO_6 and (c) RuO_6, respectively.
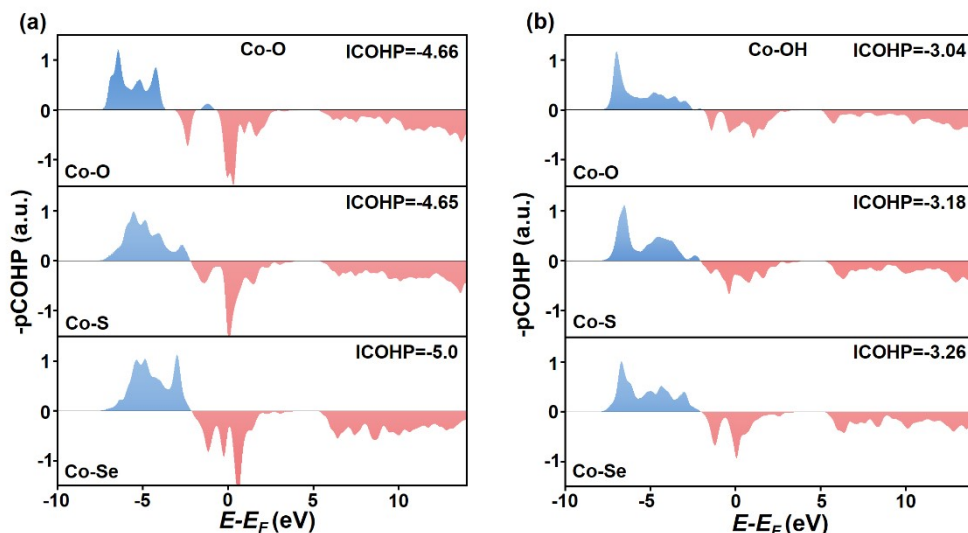
Fig. S6 Projected crystal orbital Hamilton population (pCOHP) between the Co-O and Co-OH bonds on CoO_6 units with O, S and Se ligand involved, with negative (bonding) contributions at the up position and positive (antibonding) contributions at the down position.
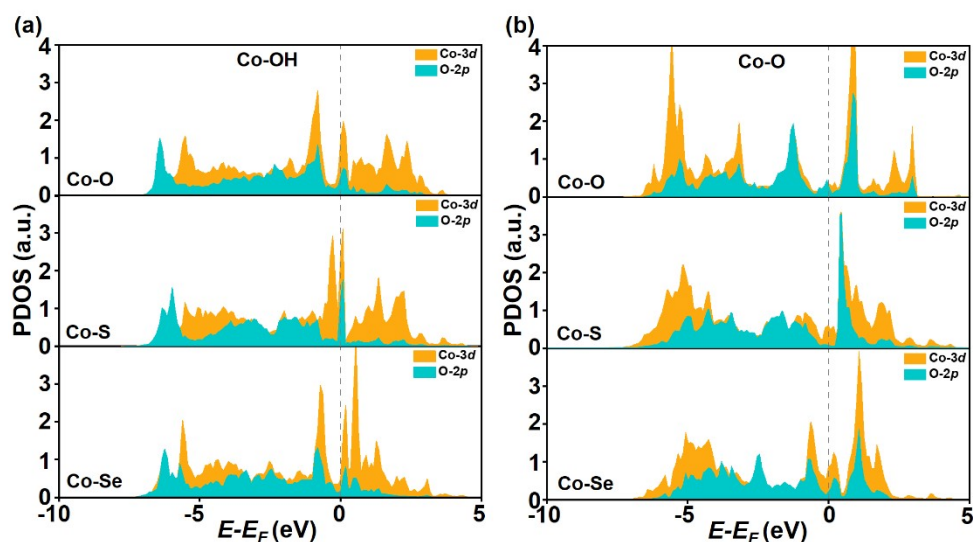
Fig. S7 Projected density of state (PDOS) for Co $3d$ in different CoO_6 units with O, S and Se ligand involved and the corresponding O $2p$ in the adsorbed *OH and *O, respectively.

To clearly illustrate and understand the different performance of the CoO_6 units with O, S and Se ligand heteroatoms incorporated in MnO_2, we conducted the detailed electronic structure analysis for them. First, we performed the projected crystal orbital Hamilton population (pCOHP) to quantitatively analyse the interaction between Co site and the key intermediate (*OH and *O) in the rate-determining step (*OH → *O + H$^+$/e$^-$). As shown in Fig. S6, compared with the pure CoO_6, it can be found that the introduction of S ligand changes the Co-O and Co-OH bonds, and even slightly weakens the Co-O bond, thus leading to the relatively high overpotential η to some extent. In contrast, the Se ligand can strongly change them, especially improving the interaction between the *O intermediate and the Co site. The greater degree of enhancement of the Co-O bond than the Co-

13

OH bond facilitates the rate-determining step of $*OH \rightarrow *O + H^+/e^-$. This can be rationalized by the stronger ability of the O species to capture electron than the OH species. To further understand the better role of Se ligand than O and S ones, we calculated the projected density of state (PDOS) for different CoO_6 units (Fig. S7) to examine the hybridization state between the O-containing species and Co site. From Fig. S7, one can confirm that the overlap of the Co $3d$ and O $2p$ orbitals of O and OH species in CoO_6 unit with Se involved is more than that in CoO_6 units with O or S involved, verifying the better bond strength of Co site in CoO_6 unit with Se involved and thus facilitating OER.

Table S3 Overpotential (η) of MO_6 incorporated in different rutile metal oxide substrate.

MO_6	Substrate	η
Co	CrO_2	0.79
Co	IrO_2	0.44
Co	RhO_2	0.59
Co	MnO_2	0.78
Co	RuO_2	0.40
Ni	CrO_2	1.02
Ni	IrO_2	0.93
Ni	RhO_2	0.97
Ni	MnO_2	1.20
Ni	RuO_2	0.92
Ru	CrO_2	0.65
Ru	IrO_2	0.56
Ru	RhO_2	0.64
Ru	MnO_2	0.85
Ru	RuO_2	0.59

Reference

1. G. Kresse and J. Hafner, *Phys. Rev. B*, 1993, **47**, 558.

2. G. Kresse and J. Hafner, *Phys. Rev. B*, 1994, **49**, 14251.

3. G. Kresse and J. Furthmüller, *Phys. Rev. B*, 1996, **54**, 11169.

4. G. Kresse and J. Furthmiiller, *Comp. Mater. Sci.*, 1996, **6**, 15.

5. J. P. Perdew, K. Burke and M. Ernzerhof, *Phys. Rev.* Lett., 1996, **77**, 3865.

6. G. Kresse and D. Joubert, *Phys. Rev. B*, 1999, **59**, 1758.

7. I. V. Solovyev, P. H. Dederichs and V. I. Anisimov, *Phys. Rev. B*, 1994, **50**, 16861.

8. P. Sinha, S. E. Boesch, C. Gu, R. Wheeler, A. Wilson, *J. Phys. Chem. A* 2004, **108**, 9213-9217.

9. http://webbook.nist.gov/chemistry

10. I. C. Man, H. Y. Su, F. Calle-Vallejo, H. A. Hansen, J. I. Martínez, N. G. Inoglu, J. Kitchin, T. F. Jaramillo and J. K. Nørskov, Jan Rossmeisl, *ChemCatChem*, 2011, **3**, 1159.

11. J. K. Nørskov, J. Rossmeisl, A. Logadottir, L. Lindqvist, J. R. Kitchin, T. Bligaard, H. Jónsson, *J. Phys. Chem. B*, 2004, **108**, 17886.

12. J. Rossmeisl, Z. W. Qu, H. Zhu, G. J. Kroes and J. K. Nørskov, *J. Electroanal. Chem.* 2007, **607**, 83.

13. M. Bajdich, M. García-Mota, A. Vojvodić, J. K. Nørskov and A. T. Bell, *J. Am. Chem Soc.*, 2013, **135**, 13521.